Pulse duration dependence of single-shot pulsed laser ablation of Gallium based III-V compound semiconductors

Marnix Vreugdenhil[1] and Dries van Oosten[1]

[1]Debye Institute for Nanomaterials Science and Center for Extreme Matter and Emergent Phenomena, Utrecht University, Princetonplein 1, 3584 CC Utrecht, The Netherlands

ABSTRACT

We experimentally study single-shot laser ablation of GaSb, GaAs, GaP and GaN, for laser pulse durations ranging from 200 fs to 20 ps. We find that the laser ablation threshold fluence of GaSb is almost independent of pulse duration, whereas the ablation threshold for GaN depends strongly on pulse duration. More generally we find that the larger the bandgap, the stronger the dependence of pulse duration. This is expected, as intrinsic laser absorption is mainly linear when the bandgap is small compared to the photon energy, whereas a larger bandgap requires strong field ionization. Thus a larger bandgap leads to a stronger influence of the peak intensity of the pulse and therefore a stronger dependence on the pulse duration, when compared to smaller bandgaps.

Keywords: Laser induced damage, ablation, GaSb, GaAs, GaP, GaN, heat conductivity, nonlinear absorption, pulse duration scaling, multiphoton absorption, strong field ionization

III-V compounds are extremely relevant in many electronic technologies, ranging from microwave frequency integrated circuits[1] to solid state lighting[2,3] and laser diodes.[4,5] Laser ablation of III-V semiconductors is an important topic, as laser dicing is an important technology in, for instance, solid state lighting.[6–8] From the point of view of fundamental research, it is also an interesting topic, as the bandgap of III-V semiconductors can be engineered by controlling the specific concentrations of the constituents.[9]

It is known that, for a given material, longer pulses lead to a higher ablation threshold, compared to shorter pulses.[10] This is often attributed to the fact that for long pulses (ps-ns), heat can diffuse away from the surface where the laser light is absorbed.[10,11] Thus, more energy is required to locally exceed the melting point of the material, which is usually identified as ablation threshold.[12] Furthermore, it is known that ablation plume formation can occur on ps timescales[13–15] and thus, for sub-picosecond pulses, the plume can form before heat conduction can carry heat away. This heat conductivity argument gives rise to a $\tau^{0.5}$ scaling of the ablation threshold.[10,16]

On the other hand, pulse duration also influences the laser absorption process, as a shorter pulse leads to a higher peak intensity and therefore to more strong field ionization. Depending on the material and the pulse duration regime, either the effect that the pulse duration has on strong field ionization efficiency, or the effect it has on heat conductivity, might be the dominant factor in determining the ablation threshold. Exploiting the wide range of bandgaps offered by III-V semiconductors, we can attempt to disentangle the importance of these two effects.

In this work, we present results of single-shot laser ablation experiments on GaSb, GaAs, GaP and GaN, for pulse duration ranging from 200 fs to 20 ps. We characterise the areas exposed to laser pulses by in-situ optical microscopy and optical interferometric profilometry. By analysing the crater radius as a function of the pulse energy, we determine the pulse duration dependent laser ablation threshold for all four compounds. The properties of the samples used in the experiment are listed in Tab. 1.

A simplified schematic view of the experimental setup is shown in Fig. 1. Pulses are generated by a *Light Conversion Pharos PH2-SP-1 mJ* laser. The output wavelength is 1034 nm and the pulse duration is continuously

Further author information: (Send correspondence to Marnix Vreugdenhil)
Marnix Vreugdenhil: E-mail: M.C.W.Vreugdenhil@uu.nl

Laser-Induced Damage in Optical Materials 2023, edited by Christopher Wren Carr, Detlev Ristau, Carmen S. Menoni, Michael D. Thomas, Proc. of SPIE Vol. 12726, 1272609 · © 2023 SPIE · 0277-786X · doi: 10.1117/12.2685122

Compound	GaN[9]	GaP[9]	GaAs[9]	GaSb[9]	Laser
$\mathbf{E_g}$ **(eV)**	3.44	2.26	1.42	0.73	1.20
$\lambda_\mathbf{g}$ **(nm)**	360	549	873	1698	1034
$\mathbf{E_g/E_{ph}}$	2.9	1.9	1.2	0.6	1
Thickness (mm)	0.5	0.35	0.5	0.35	
Orientation	(100)	(100)	(100)	c-plane (0001)	
$\mathbf{F_{th}}(200\ fs)(Jcm^{-2})$	0.78	0.36	0.29	0.23	
$\mathbf{F_{th}}(20\ ps)(Jcm^{-2})$	4.62	1.30	0.53	0.25	
$\mathbf{F_{max}}(Jcm^{-2})$	5.32	5.04	1.74	1.74	

Table 1. Properties (at 300 K) of the III-V samples used in this work as well as the photon energy of the laser that we use for our experiments. The row marked λ_g shows the wavelength of light corresponding to the bandgap energy. Ablation threshold fluences at pulse durations of 200 fs and 20 ps, respectively, are shown in the rows marked with $\mathbf{F_{th}}$. These values all have an error smaller than 2.5%. The bottom row shows the highest fluence to which we have exposed each sample during each run.

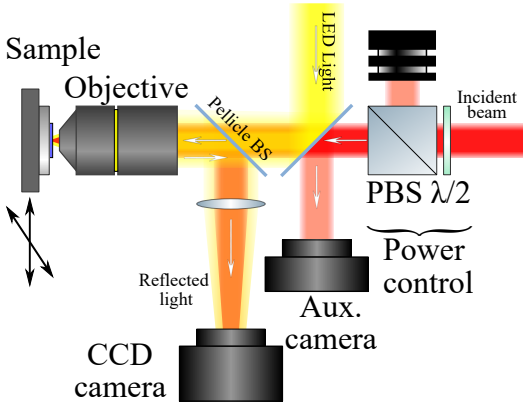

Figure 1. Simplified schematic representation of the experimental setup.

tunable from 200 fs up to 20 ps. We control the pulse energy, using a motorized half wave plate and a polarizing beam splitter. Neutral density filters are used to choose an energy range most suitable for the material under study. After passing two pellicle beamsplitters, oriented at $+45°$ and $-45°$ respectively, pulses are focused on the sample surface, using a microscope objective (Nikon CFI60, 100×, NA = 0.8). The sample is mounted on a motorized stage. For each shot during an experiment, we record an image before, during and after the exposure as well as an image of the incident laser pulse (acquired using a beam splitter and an auxiliary camera) to determine the pulse energy on a single shot basis. A single experiment consist of 64 runs. During each run, we expose the sample to 64 individual laser shots. Between each exposure, the pulse energy is changed and the sample is moved such that each time, a fresh piece of sample is exposed. After every 4 runs, we change the compressor settings of the laser in order to increase the pulse duration. For reference, the samples are analysed in an optical profilometer to obtain the surface topography of the resulting craters. This experiment is repeated for the four samples over the course of three days. The reproducibility of our experiments is very high and we gather large amounts of data over the course of a single experiment. More details on the setup and on the data management and analysis workflow are described in reference.[17]

All data used in this publication are available online at (citation). Appendix A includes a description on how to navigate our data and scripts.

Typical aftermath microscopy images are shown in Fig.2, for GaSb (top row) and GaN (bottom row) at a pulse duration of 200 fs (left column) and 16 ps (right column). Note that the pulse energy range used for GaN and GaSb are not identical (as GaN has a much higher ablation threshold than GaSb, see Tab. 1), but in either case, the pulse energy range for the different pulse duration is identical. We can therefore immediately see that, for GaSb, the sub-image in which we first observe damage hardly changes when we go from a pulse duration of 200 fs to 16 ps. In contrast, for GaN, there is a dramatic difference between these two extremes in pulse duration.

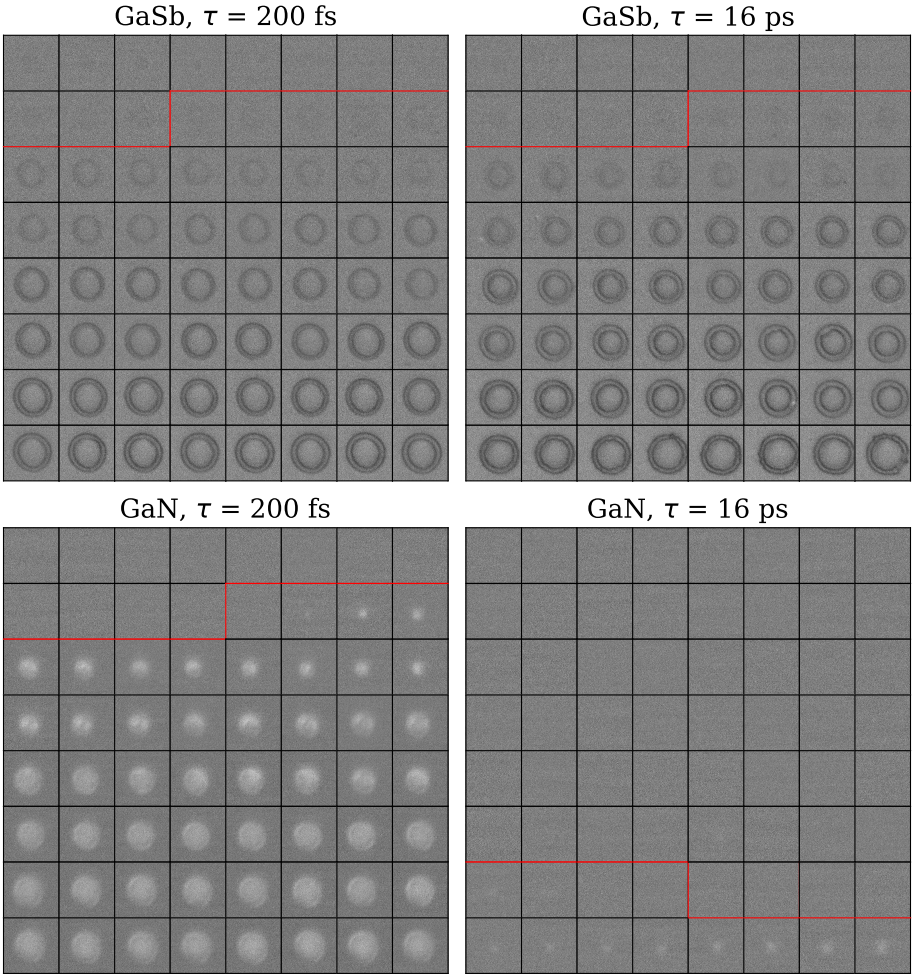

Figure 2. Example in-situ images of the aftermath, for GaSb illuminated with 200 fs pulses (a) and 16 ps pulses (b) and for GaN illuminated with 200 fs pulses (c) and 16 ps pulses (d). In each of these subplots, the pulse energy increases in a meandering fashion, meaning that the energy increases from right to left in the first row, from left to right in the second row, and so on. The red line separates the regime below the ablation threshold from the regime above it.

To make a more quantitative statement about the ablation threshold, we carry out a Liu analysis.[18] This analysis is based on the assumption that there is a single threshold fluence F_{th} above which a damage process occurs. If we assume the (time integrated) spatial fluence profile $F(r)$ of the laser focus to be Gaussian,

$$F(r) = \sqrt{\pi}\tau I_0 \exp\left(\frac{-r^2}{2w_0^2}\right) = F_0 \exp\left(\frac{-r^2}{2w_0^2}\right), \tag{1}$$

where I_0 is the intensity at the center of the beam, r is the distance from the center and w_0 is the waist of the beam and the threshold fluence $F_{th} = F(r_{th})$, then

$$r_{th}^2 = 2w_0^2 \left(\log F_0 - \log F_{th}\right). \tag{2}$$

This relation holds for any fluence for which $F_0 > F_{th}$. Note that F_0 scales linearly with the pulse energy.

We determine the radius of each crater by analyzing the radial profiles around the center of each crater of the microscope images of the sites. After determining the crater radii, we plot the square of the radii as a function of the logarithm of the pulse energy. We fit a linear function to the part of the curve that is a straight line, since we expect Eq. 2 to hold. The slope of the line is a measure for the focus waist and the intercept with the x-axis

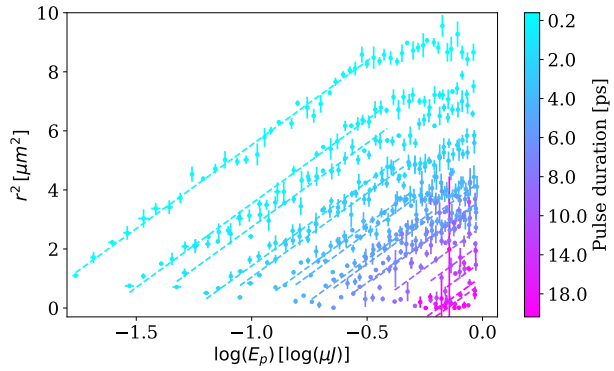

Figure 3. Liu analysis for GaN. The squared crater radius, extracted from microscopy images, is plotted as a function of the natural logarithm of the pulse energy, for several pulse durations. A linear function is fitted to the data for each pulse duration (dashed lines). The slope for all pulse durations is kept the same, whereas the offset is adjusted separately. The intercept with the x axis yields the threshold energy.

yields the ablation threshold fluence. As an example, we show this analysis for GaN in Fig. 3; the different colors corresponding to different pulse durations. Note that during the fitting, we use the same slope for each pulse duration, as we have verified that the beam shape does not change significantly when we vary the compressor settings of the laser and the focus waist should thus not depend on pulse duration.

To independently verify that the threshold fluences that we extract from the Liu analysis are accurate, we make use of the topography profiles that we measured using optical profilometry. In Fig. 4, we plot the depth of the craters as a function of the fluence, normalized to the corresponding threshold fluence. For each data point, we take a weighted average of the (four) craters taken under identical conditions. We observe that for all compounds and all pulse durations, the crater starts forming at a normalized fluence of 1, as expected.

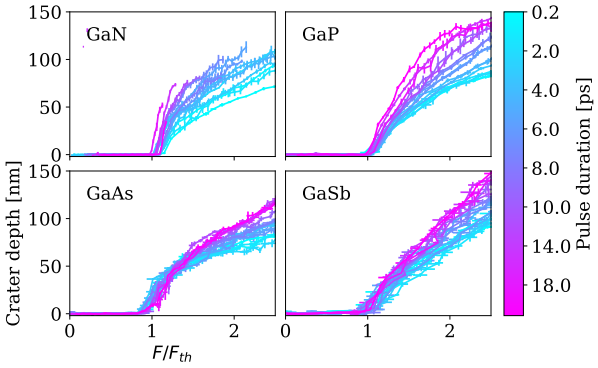

Figure 4. Weighted average depths of all craters as a function of the pulse fluence normalized to the corresponding threshold fluence, determined using optical profilometry.

We summarize the results of the Liu-analyses for all samples in Fig.5. Here, the different colors correspond to the different samples.

From Fig. 5, we see that, as we already qualitatively learned from Fig. 2, the ablation threshold of GaSb does not depend significantly on laser pulse duration, whereas the ablation threshold of GaN shows a pronounced dependence. The other samples show an intermediate behaviour and it appears that the dependence becomes stronger with increasing bandgap. We observe that GaN shows a bimodal behaviour. For small pulse duration, the ablation threshold seems to approach a constant and for large duration it approaches a rising straight line, which points to a power law dependence on pulse duration.

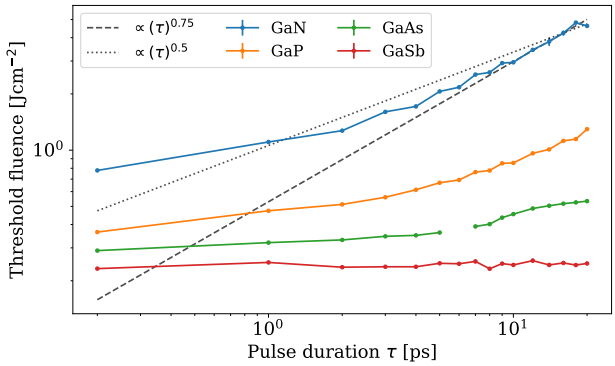

Figure 5. Threshold energy obtained from a Liu analysis of the crater radius, as a function of pulse duration, for several Gallium based III-V compound semiconductors. The dashed and dotted gray lines are guides to the eye corresponding to power laws of 0.75 and 0.5, respectively.

As a guide to the eye, we have included lines corresponding to power laws of 0.75 (dashed line) and 0.5 (dotted line). Although the range of pulse durations available to us in the experiment does not allow us to conclude the correct power law, it is clear that we can exclude the power 0.5. As mentioned earlier, this square-root dependence is derived on the assumption that heat conductivity is the dominating factor determining the increase in ablation threshold. However, it is not apparent that heat conduction should affect these different compounds so dramatically differently as to explain the difference in behaviour. Furthermore, the square-root behavior is usually discussed in the ps-ns pulse duration regime. As we used pulses with a fs-ps pulse duration, it is perhaps unsurprising that we do not observe this square root behaviour in our experiment.

We conclude from the above that heat conductivity is likely not the governing factor in determining the pulse duration dependence of the threshold fluence and we therefore rather attribute the behaviour to the difference in light absorption; *i.e.* by the fact that a larger bandgap requires a higher order nonlinear absorption and therefore will show a stronger dependence of peak intensity rather than total fluence. The exact role of the influence of the strong field ionization coefficients and thermal effect on the pulse duration dependence of these compounds requires further study.

To summarize, we have done extensive single-shot ablation experiments on GaSb, GaAs, GaP and GaN. More specifically, we have studied the pulse-duration dependence of the ablation threshold fluences of these compounds for pulse durations ranging from 200 fs up to 20 ps. We have found that the pulse duration scaling of the thresholds depends very strongly on the band gap of the material. When the band gap is small compared to the photon energy of the laser pulses used, the ablation threshold does not scale with pulse duration. If the band gap is large, on the other hand, the threshold fluence scales strongly with pulse duration, approaching a power law of ≈ 0.75 for large pulse durations in the case of GaN. These dependencies differ significantly from the often discussed $\tau^{0.5}$.

APPENDIX A. DATA MANAGEMENT

The python scripts used to generate the figures that we present in the main text are publicly available online in a DOI minted vault. Here, one can also access all raw data, processing scripts, analysis scripts and processed data. All raw data are located in the base folder corresponding to the date when the data were acquired. The date that the in-situ data were acquired does not necessarily correspond to the date that the optical profilometry data were acquired, as these measurements could have been done on different days. Tab. 2 shows an overview of the base folders in which the raw data for different samples are stored. Raw data are always located in the *Data/RawData/* subfolder of the base folder shown in the table. All pre-processing scripts for raw data are located in the *PreProcessing/* subfolder of this base folder.* Scripts for converting the crater radii from pixels

*That means that the pre-processing scripts for the aftermath data of GaSb are in *20211118/PreProcessing/*, but the pre-processing scripts for the profilometry data of the same sample are located in *20211119/PreProcessing/*.

	GaN	GaP	GaAs	GaSb
Aftermath data	20211117	20211119	20211119	20211118
Optical profilometry	20211118	20211122	20211119	20211119
First run	72	64	0	1
Last run	135	127	63	64

Table 2. Overview of the base folders in which data and processing files are located for each sample.

to μm and scripts for finding the depth of the craters are located in the Analysis/ subfolders. There are two other base folders: *InfluenceOfBandgap/* and *APL_2022_ManuscriptFigures/*. *InfluenceOfBandgap/* includes the scripts that execute the Liu analysis. Finally, as the name implies, *APL_2022_ManuscriptFigures/* contains all the scripts that generate the figures that are shown in the main text. These scripts are an excellent starting point to navigate the data set.

ACKNOWLEDGMENTS

The authors thank Javier Hernandez Rueda, Ester Abram and Vina Faramarzi for careful reading of the manuscript and Paul Jurrius, Dante Killian, Aron Opheij and Cees de Kok for technical support.
This publication is part of the project "Wafer damage control: understanding and preventing light-induced material changes in optical measurement systems" (with project number 17963) of the research programme High Tech Systems and Materials (HTSM) which is (partly) financed by the Dutch Research Council (NWO). The project is co-financed by ASMPT ALSI and ASML.

REFERENCES

[1] Fan, J. C., "Thin films of iii-v compounds and their applications," *J. Phys. Colloques* **43**(C1), C1–327–C1–339 (1982).

[2] Krames, M. R., Shchekin, O. B., Mueller-Mach, R., Mueller, G. O., Zhou, L., Harbers, G., and Craford, M. G., "Status and future of high-power light-emitting diodes for solid-state lighting," *Journal of Display Technology* **3**(2), 160–175 (2007).

[3] Nakamura, S., "Current status of gan-based solid-state lighting," *MRS Bulletin* **34**(2), 101–107 (2009).

[4] Fasol, G., "Room-temperature blue gallium nitride laser diode," *Science* **272**(5269), 1751–1752 (1996).

[5] Milnes, A. and Polyakov, A., "Gallium antimonide device related properties," *Solid-State Electronics* **36**(6), 803–818 (1993).

[6] Roelkens, G., Liu, L., Liang, D., Jones, R., Fang, A., Koch, B., and Bowers, J., "Iii-v/silicon photonics for on-chip and intra-chip optical interconnects," *Laser & Photonics Reviews* **4**(6), 751–779 (2010).

[7] Wasmer, K., Ballif, C., Pouvreau, C., Schulz, D., and Michler, J., "Dicing of gallium–arsenide high performance laser diodes for industrial applications: Part i. scratching operation," *Journal of Materials Processing Technology* **198**(1), 114–121 (2008).

[8] Gu, E., Jeon, C., Choi, H., Rice, G., Dawson, M., Illy, E., and Knowles, M., "Micromachining and dicing of sapphire, gallium nitride and micro led devices with uv copper vapour laser," *Thin Solid Films* **453-454**, 462–466 (2004). Proceedings of Symposium H on Photonic Processing of Surfaces, Thin Films and Devices, of the E-MRS 2003 Spring Conference.

[9] Kasap, S. O. and Capper, P., [*Springer handbook of electronic and photonic materials*], vol. 11, Springer (2006).

[10] Gamaly, E. G., Rode, A. V., Luther-Davies, B., and Tikhonchuk, V. T., "Ablation of solids by femtosecond lasers: Ablation mechanism and ablation thresholds for metals and dielectrics," *Physics of Plasmas* **9**(3), 949–957 (2002).

[11] Ristau, D., [*Laser-induced damage in optical materials*], CRC Press (2014).

[12] Rämer, A., Osmani, O., and Rethfeld, B., "Laser damage in silicon: Energy absorption, relaxation, and transport," *Journal of Applied Physics* **116**(5), 053508 (2014).

[13] Hernandez-Rueda, J. and van Oosten, D., "Dynamics of ultrafast laser ablation of water," *arXiv preprint arXiv:1810.06946* (2018).

[14] Vreugdenhil, M., van Oosten, D., and Hernandez-Rueda, J., "Dynamics of femtosecond laser-induced shock-waves at a water/air interface using multiple excitation beams," *Opt. Lett.* **43**, 4899–4902 (Oct 2018).

[15] Wood, R., Leboeuf, J., Chen, K., Geohegan, D., and Puretzky, A., "Dynamics of plume propagation, splitting, and nanoparticle formation during pulsed-laser ablation," *Applied Surface Science* **127-129**, 151–158 (1998).

[16] Feit, M. D. and Rubenchik, A. M., "Implications of nanoabsorber initiators for damage probability curves, pulselength scaling, and laser conditioning," in [*Laser-Induced Damage in Optical Materials: 2003*], Exarhos, G. J., Guenther, A. H., Kaiser, N., Lewis, K. L., Soileau, M. J., and Stolz, C. J., eds., **5273**, 74 – 82, International Society for Optics and Photonics, SPIE (2004).

[17] Vreugdenhil, M. and van Oosten, D., "A highly automated apparatus for ultra-fast laser ablation studies," *Review of Scientific Instruments* **93**(7), 073003 (2022).

[18] Liu, J. M., "Simple technique for measurements of pulsed gaussian-beam spot sizes," *Opt. Lett.* **7**, 196–198 (May 1982).